

1 **A genetic particle filter scheme for univariate data assimilation**
2 **into Noah-MP model across snow climates**

3 Yuanhong You^a, Chunlin Huang^b, Zuo Wang^a, Jinliang Hou^b, Ying Zhang^a, Peipei Xu^b

4
5 ^aCollege of Geography and Tourism, Anhui Normal University, Wuhu, 241002, China

6
7 ^bNorthwest Institute of Eco-Environment and Resources, Chinese Academy of Sciences, Lanzhou,
8 730000, China

9
10
11
12
13
14
15
16
17
18
19
20
21

Corresponding author: Chunlin Huang, Key Laboratory of Remote Sensing of Gansu Province,
Northwest Institute of Eco-Environment and Resources, Chinese Academy of Sciences, Lanzhou,
Gansu, 730000, China. (huangcl@lzb.ac.cn)

Submitted to: Hydrology and Earth System Sciences
March, 2023

22 **Abstract**

23 Accurate snowpack simulations are critical for regional hydrological predictions, snow
24 avalanche prevention, water resource management, and agricultural production, particularly during
25 the snow ablation period. Data assimilation methodologies are increasingly being applied to
26 operational purposes to reduce the uncertainty in snowpack simulations and enhance their predictive
27 capabilities. This study aims to investigate the feasibility of using Genetic Particle Filter (GPF) as a
28 snow data assimilation scheme designed to assimilate ground-based snow depth (SD) measurements
29 across different snow climates. We employed the default parameterization scheme combination
30 within the Noah-MP model as the model operator in the snow data assimilation system to evolve
31 snow variables and evaluated the assimilation performance of GPF using observational data from the
32 sites with different snow climates. We also explored the impact of measurement frequency and
33 particle number on the filter updating of the snowpack state at different sites and compared the results
34 of generic resampling methods with the genetic algorithm used in the resampling process. Our results
35 demonstrate that GPF can be used as a snow data assimilation scheme to assimilate ground-based
36 measurements and obtain satisfactory assimilation performance across different snow climates. We
37 found that particle number is not crucial for the filter's performance, and 100 particles are sufficient
38 to represent the high dimensionality of the point-scale system. The frequency of measurements can
39 significantly affect the filter updating performance, and dense ground-based snow observational data
40 always dominates the accuracy of assimilation results. Compared to generic resampling methods, the
41 genetic algorithm used to resample particles can significantly enhance the diversity of particles and
42 avoid particle degeneration and impoverishment. Finally, we concluded that the GPF is a suitable
43 candidate approach to snow data assimilation and is appropriate for different snow climates.

44 **1. Introduction**

45 Understanding snowpack dynamics is crucial for water resource management, agricultural
46 production, avalanche prevention and flood preparedness in snow dominated regions (Piazzini et al.,
47 2019; Pulliainen et al., 2020). As a special land surface type, seasonal snow cover is highly sensitive
48 to climate change and has a significant impact on energy and hydrological processes (Barnett et al.,
49 2005; Takala et al., 2011; Kwon et al., 2017; Che et al., 2014). On one hand, the high snow surface
50 albedo can significantly reduce shortwave radiation absorption, leading to adjustments in the energy
51 exchange between the land surface and atmosphere (You et al., 2020a; You et al., 2020b). On the
52 other hand, the low thermal conductivity of snow cover can insulate the underlying soil, resulting in
53 reduced temperature variability and a more stable condition (Zhang et al., 2005; Piazzini et al., 2019).
54 Additionally, snowmelt is an important water resource that plays a critical role in soil moisture, runoff,

55 and groundwater recharge (Dettinger, 2014; Griessinger et al., 2016; Oaida et al., 2019). Consequently,
56 understanding snow dynamics is crucial for predicting snowmelt runoff, atmospheric circulation,
57 hydrological predictions, and climate change.

58 Currently, there is a growing effort to investigate the potential of data assimilation (DA) schemes
59 to improve snow simulations and obtain the optimal posterior estimate of the snowpack state
60 (Bergeron et al., 2016; Piazzini et al., 2018; Smyth et al., 2020; Abbasnezhadi et al., 2021). Various DA
61 methodologies with different degrees of complexity have been developed, resulting in diverse
62 performance levels. Sequential DA techniques, including basic direct insertion, optimal interpolation
63 schemes, ensemble-based Kalman filter, and particle filter, have been widely employed in real-time
64 applications. The greatest strength of sequential DA techniques is that the model state can be
65 sequentially updated when observational data become available (Piazzini et al., 2018). However, the
66 direct insertion method, which replaces model predictions with observations when available, is based
67 on the assumption that the observation is perfect and the model prior is wrong (Malik et al., 2012).
68 This method can potentially result in model shocks due to physical inconsistencies among state
69 variables (Magnusson et al., 2017). Although the optimal interpolation method is more advanced and
70 takes into account observational uncertainty, it still has great limitations and is rarely used in real-
71 time operational systems (Dee et al., 2011; Balsamo et al., 2015).

72 At a higher level are the Kalman filter and ensemble-based Kalman filter, which are most
73 commonly used in various real-time applications. The Ensemble Kalman Filter (EnKF), which was
74 first introduced by Evensen in 2003, uses a Monte Carlo approach to approximate error estimates
75 based on an ensemble of model predictions. This approach does not require model linearization,
76 making it particularly advantageous. Precisely due to this advantage, the EnKF has been widely used
77 in snowpack prediction. For example, EnKF has been used to assimilate MODIS snow cover extent
78 and AMSR-E SWE into a hydrologic model to improve modeled SWE (Andreadis et al., 2006), as
79 well as to assimilate MODIS fractional snow cover into a land surface model (Su et al., 2008).
80 Moreover, the EnKF method has been used to enhance snow water equivalent estimation by
81 assimilating ground-based snowfall and snowmelt rates, simultaneous assimilation of D-InSAR,
82 automatically and manually measured snow depth data (Yang and Li, 2021). Even though there are
83 numerous studies generally stated that the EnKF has an excellent assimilation performance enabling
84 to consistently improve snow simulations, some constraining limitations hinder the filter performance
85 (Chen, 2003). One of the main limitations is that the EnKF assumes that the model states follow a
86 Gaussian distribution and only considers the first and second order moments, thereby losing relevant
87 information contained in higher-order moments (Moradkhani et al., 2005). Unfortunately, the
88 dynamic system usually has strong nonlinearity and the involved probability distribution of system
89 state variables are not supposed to follow a Gaussian distribution (Weerts and El Serafy, 2006).
90 Additionally, the filter performance of the EnKF is significantly influenced by the linear updating

91 procedure, and the state-averaging operations can be particularly challenging for highly detailed
92 complex snowpack models.

93 In order to overcome these limitations, the particle filter (PF) which also based on Monte Carlo
94 method has been developed for non-Gaussian, nonlinear dynamic models (Gordon et al., 1993). The
95 greatest strength of PF technique is free from the constraints of model linearity and error following
96 Gaussian distribution, this makes the PF technique succeed applied in nonlinear and non-Gaussian
97 dynamic systems. Additionally, PF technique give weights to individual particles but leave model
98 states untouched, which makes PF more computationally efficient than ensemble Kalman filter and
99 smoother (Margulis et al., 2015). Thanks to these advantages, an increasing interest focuses on
100 applying PF technique in snow data assimilation. For example, remotely sensed microwave radiance
101 data was assimilated into snow model for updating model states by PF technique, and the results
102 demonstrated that the SWE simulations have great improvement (Dechant and Moradkhani, 2011;
103 Deschamps-Berger et al., 2022). A newly PF approach proposed by Margulis et al. (2015) was used
104 to improve SWE estimation through assimilating remotely sensed fractional snow-covered area. At
105 basin scale, PF technique was implemented with the objective of obtaining high resolution
106 retrospective SWE estimates (Cortes et al., 2016). The PF technique was also used to assimilate daily
107 snow depth observations within a multi-layer energy-balance snow model to improve SWE and
108 snowpack runoff simulations (Magnusson et al., 2017). Above studies demonstrated that either
109 assimilated the snow-related in-situ measurements or remotely sensed observation data through PF
110 technique can successfully update the predictions of snowpack dynamics, and the PF scheme is a
111 well-performing data assimilation technique enabling to consistently improve model simulations.
112 Nevertheless, particle degeneracy is still one potential limitation for PF technique, it occurs when
113 most of particles have negligible weight and only few particles have significant weights, which makes
114 the state probability distribution cannot be represented by the particles (Parrish et al., 2012;
115 Abbaszadeh et al., 2017; Abbaszadeh et al., 2018). The particle resampling has been considered to be
116 an efficient approach which can effectively mitigate the problem of particle degeneracy, however, it
117 may lead to the resulting sample will contain many repeated points and a lack of diversity among the
118 particles, which is defined sample impoverishment (Rings et al., 2012; Zhu et al., 2018). And the
119 sample impoverishment was a tricky problem for generic resampling methods. Using intelligent
120 search and optimization methods to mitigate the degeneracy problem may be a good choice since it
121 can avoid the sample impoverishment well (Park et al., 2009; Ahmadi et al., 2012; Abbaszadeh et al.,
122 2018). The Genetic Algorithm (GA) as an intelligent search and optimization method has been known
123 as an effective approach to mitigate the degeneracy problem and received more attention (Kwok et
124 al., 2005; Park et al., 2009; Mechri et al., 2014). The GA applied in particle filter, which is defined
125 genetic particle filter (GPF), has been successfully implemented to estimate parameters or states in
126 nonlinear models (Van Leeuwen, 2010; Snyder, 2011). The GPF was also used as data assimilation

127 scheme applied to land surface model which simulates prior subpixel temperature and the results
128 showed the GPF outperformed prior model estimations (Mechri et al., 2014). Despite a series of
129 studies have proved that the GPF is an effective data assimilation approach, however, few studies
130 have investigated the performance of GPF as a snow data assimilation scheme, especially in different
131 snow climates. In view of the promising performances of GPF as a snow data assimilation scheme,
132 this paper aims to investigate the potential of GPF in performing snow data assimilation, and the main
133 goal of this research is to address the following issues: (1) Can the GPF be employed as a snow data
134 assimilation scheme? (2) How is the assimilation performance of GPF in snow data assimilation
135 across different snow climates? (3) The sensitivity of DA simulations to the frequency of the
136 assimilated measurements and the particle number.

137 This paper is organized as follows. Section 2 introduces the information of study sites, the
138 meteorological dataset, the snow module within the Noah-MP model, calculation flow of GPF scheme,
139 and design of numerical experimental. Section 3 explains the simulation results of SD by open-loop
140 ensemble, explores the sensitivity of measurement frequency and ensemble size. Section 4
141 summarizes the findings of this study.

142 **2. Materials and methods**

143 *2.1 Study sites and data*

144 With the consideration of the filtering performance maybe diverse in snow climates, eight
145 seasonally snow-covered study sites with different snow climates in total were selected to implement
146 numerical experimental in this study (Sturm et al., 1995; Trujillo and Molotch, 2014). These sites are
147 distributed at different latitudes in the northern hemisphere, and the sites included the Arctic
148 Sodankylä site (SDA, 179 m), located beside the Kitinen River in Finland and has a 2 m depths soil
149 frost (Rautiainen et al., 2014); the Snoqualmie site (SNQ, 921 m) with a rain-snow transitional climate
150 in the Washington Cascades of the USA, in this site, the SD measured from snow stakes was employed
151 (Wayand et al., 2015); the maritime Col de Porte (CDP, 1330 m) site in the Chartreuse Range in the
152 Rhone-Alpes of France; the Mediterranean climate Refugio Poqueira site (ROPA, 2510 m) in Sierra
153 Nevada Mountains of Spain and has a high evaporation rate (Herrero et al., 2009); the Weissfluhjoch
154 site (WFJ, 2540 m) in Davos of Switzerland, and automatic observations of SD were used in this
155 study (Wever et al., 2015); the continental Swamp Angel Study Plot (SASP, 3370 m) site in the San
156 Juan Mountains of Colorado, USA; and two sites from typical snow-covered regions in China, the
157 Altay meteorological observation site (ATY, 735.3 m) in Northern Xinjiang, China, which has less
158 wind in the winter season; the other one is the Mohe meteorological observation site (MOHE, 438.5
159 m) in a county of Northeast China, which is the northernmost part of China and has a cold temperate
160 continental climate. Serially complete meteorological measurements are available and can be used as

161 forcing data in these sites, certainly, the downward longwave and shortwave radiation values of
 162 MOHE were extracted from the China Meteorological Forcing Dataset (CMFD) (Chen et al, 2011),
 163 since there are no radiation measurements in this site.

164 It is noteworthy that the spatial variance on the performance of the model is negligible since
 165 these sites themselves are flat and surrounding vegetation types are uniform. We have used this data
 166 set to examine the sensitivity of simulated SD to physics options, and the results showed that the
 167 dataset has a reliable quality. In addition, the location, detailed information of snow climates, and
 168 dataset process introduction of the eight sites can be also referenced in You et al. (2020a).

169 **2.2 Snow module within Noah-MP model**

170 The snow partial within Noah-MP model can be divided into three layers at most according to
 171 snow depth (Yang et al., 2011). The SD h_{snow} is calculated by

$$172 \quad h_{snow}^t = h_{snow}^{t-1} + \frac{P_{s,g}}{\rho_{sf}} dt . \quad (1)$$

173 where $P_{s,g}$ is the snowfall rate at the ground surface, dt is the timestep, and ρ_{sf} is the bulk
 174 density of the snowfall. When $h_{snow} < 0.025$ m, the snowpack is combined with the top soil layer and
 175 there are no dependent snow layer exists. When $0.025 \leq h_{snow} \leq 0.05$ m, the snow layer is created with
 176 the thickness equal to SD. When $0.05 < h_{snow} \leq 0.1$ m, the snowpack will be divided into two layers and
 177 both thickness $\Delta z_{-1} = \Delta z_0 = h_{snow} / 2$. When $0.1 < h_{snow} \leq 0.25$ m, the thickness of first layer is $\Delta z_{-1} = 0.05$ m
 178 and the thickness of second layer is $\Delta z_0 = (h_{snow} - \Delta z_{-1})$ m. When $0.25 < h_{snow} \leq 0.45$ m, a third layer is
 179 created and the three thickness are: $\Delta z_{-2} = 0.05$ m and $\Delta z_{-1} = \Delta z_0 = (h_{snow} - \Delta z_{-2}) / 2$ m. When $h_{snow} > 0.45$
 180 m, the layer thickness of the three snow layers are $\Delta z_{-2} = 0.05$ m, $\Delta z_{-1} = 0.2$ m,
 181 $\Delta z_0 = (h_{snow} - \Delta z_{-2} - \Delta z_{-1})$ m. Certainly, the snow cover is highly influenced by air and ground
 182 temperature, snow layer is combined with the neighboring layer since sublimation or melt, and be
 183 redivided depending on the total SD. The snow module of Noah-MP model provides an estimate of
 184 snow-related variables using energy and mass balance which computing process requires a series of
 185 meteorological forcing data such as, near surface air temperature, precipitation, and downward solar
 186 radiation. Snow accumulation or ablation parameterization of the Noah-MP model is based on the
 187 mass and energy balance of the snowpack, and the snow water equivalent can be calculated by
 188 following equation:

189
$$\frac{dW_s}{dt} = P_{s,g} - M_s - E . \quad (2)$$

190 where W_s is the snow water equivalent (mm), $P_{s,g}$ is the solid precipitation (mm s^{-1}), M_s is the
 191 snowmelt rate (mm s^{-1}), E is the snow sublimation rate (mm s^{-1}).

192 A snow interception model was implemented into Noah-MP model to describe the process of
 193 snowfall intercepted by the vegetation canopy (Niu and Yang, 2004). Within this model, the snowfall
 194 rate at the ground surface $P_{s,g}$ is then calculated by

195
$$P_{s,g} = P_{s,drip} + P_{s,throu} . \quad (3)$$

196 where $P_{s,drip}$ (mm s^{-1}) is the drip rate of snow, $P_{s,throu}$ (mm s^{-1}) is the through-fall rate of snow. In
 197 Noah-MP model, the ground surface albedo is parameterized as an area-weighted average of albedos
 198 of snow and bare soil, and the snow cover fraction of the canopy was used to calculate the ground
 199 surface albedo. As in the equation (4),

200
$$\alpha_g = (1 - f_{snow,g}) \alpha_{soil} + f_{snow,g} \alpha_{snow} . \quad (4)$$

201 where α_{soil} and α_{snow} are the albedo of bare soil and snow, respectively. $f_{snow,g}$ is the snow cover
 202 fraction on the ground and parameterized as a function of snow depth, ground roughness length and
 203 snow density (Niu and Yang, 2006).

204 **2.3 Genetic particle filter data assimilation scheme**

205 The Bayesian recursive estimation problem is solved by the Monte Carlo approach within PF
 206 technique, making this scheme is appropriate for nonlinear system with a non-gaussian probability
 207 distribution (Magnusson et al., 2017). The basic concept of PF technique is to use a large number of
 208 random realizations (i.e., particles) of the system state to represent the posterior distribution,
 209 meanwhile, the particles are propagated forward in time as the model evolved. The weights associated
 210 with the particles are updated based on the likelihood of each particle's simulated proximity to the
 211 real observation, and the weight of the particles can be updated as follows:

212
$$w_t^i = w_{t-1}^i p(z_t | x_t^i) . \quad (5)$$

213 where w_{t-1}^i is the weight of i th particle at time $t-1$ and the weight is updated by the likelihood
 214 function $p(z_t | x_t^i)$, which measures the likelihood of a given model state with respect to the
 215 observation z_t . In general, a Gaussian distribution was assumed to perturb the observations and the
 216 likelihood function was defined to represent the errors. In this study, we employed a normal

217 probability distribution to serve as likelihood function:

$$218 \quad p(z_t | x_t^i) = N(z_t - x_t^i, \sigma). \quad (6)$$

219 where N represents the normal probability distribution of the residuals between observed, z_t , and
220 simulated, x_t . Finally, the weights of the updated model state would be normalized, and the
221 assimilated value of model state is the weighted average of all particles at time t . Although the
222 particle filter has been widely applied in various nonlinear systems, the particle degeneracy and
223 impoverishment in particle filter are still the fatal limitations need to be urgently addressed. To
224 address the degeneration problem in PF technique, traditional resampling methods like multinomial
225 resampling, systematic resampling were employed to resample the particles if the effective sample
226 size,

$$227 \quad N_{eff} = 1 / \sum_{i=1}^N (w_t^i)^2. \quad (7)$$

228 fell below a specified number. To be honest, the traditional resampling methods can effectively
229 mitigate the particle degeneracy problem by resampling high-quality particles, however, it will leads
230 to the particles lack of diversity seriously after multiple iterations, that is the so-called particle
231 impoverishment problem. For the sake of mitigating these two problems simultaneously, we
232 employed the genetic algorithm (GA) to resample the particles, and this is the genetic particle filter
233 algorithm (GPF). The GA was inspired by Darwin's evolution theory and emphasizes the principle of
234 the survival of the fittest, in fact, the "fitness" of particles should be reselected in the resampling
235 phase according to the theory of particle filter. The selection, crossover and mutation are major steps
236 to simulate population evolution, as shown in Figure 1, we used the three operators to produce better
237 offspring and improve the whole population fitness, which was expected to prevent particle
238 degeneracy and impoverishment. These three operators will be used to improve the particle fitness
239 when the fitness less than a threshold value. The three operators are described as below.

240 **Selection mechanism:** At the time of assimilation, the selection operator will preferentially select the
241 particles which close to the observed SD. This process is usually achieved by sorting the fitness value
242 of all particles and selecting a certain proportion of particles. Here, we calculated the survival rate of
243 all individuals and sorted them in ascending order, the top fifth percentile of particles were considered
244 as high-quality particles and were selected as parents in genetic algorithm. This can ensure the fitness
245 individuals can be delivered to next generation group. The survival rate of particles can be calculated
246 by following equation:

$$247 \quad P(x_{t,i}) = \exp \left[-\frac{1}{R_k} (x_{i,k|k-1} - z_k)^2 \right]. \quad (8)$$

248 where R_k is the observation error at time k , 0.01 m was set in this study; z_k represents the

249 observed SD.

250 **Crossover mechanism:** The purpose of crossover operator is to exchange some genes for two or
251 more chromosomes in a specified way to form new individuals. GA mainly generates new individuals
252 by this way, which also determines the capability of global search. In this study, the arithmetic
253 crossover method was used to generate new individuals and play the role of crossover operator.
254 Selecting two particles randomly from the resampled particle group and combining them linearly to
255 form a new particle. Assumed the two selected particles are $\{x_m, x_n\}$, and the new particles were
256 formed by following equations:

$$257 \quad x'_m = \alpha x_m + (1 - \beta) x_n. \quad (9)$$

$$258 \quad x'_n = \beta x_n + (1 - \alpha) x_m. \quad (10)$$

259 where α , β are the empirical crossover coefficients, and $\alpha = 0.45$, $\beta = 0.55$ in this study. In
260 order to ensure the diversity of particles, the new formed particles will be abandoned when the
261 $x'_m = x'_n$ occurred, and the parent individuals will be re-selected from the particle group.

262 **Mutation mechanism:** The mutation in GA refers to replacing the gene values at some loci with
263 other alleles to form a new individual. The mutation mechanism can be considered as a supplement
264 to the crossover mechanism which can increase the diversity of the population. Assuming that the
265 randomly selected particle from the crossed particle set is, the mutation operation is performed on the
266 particle by the following equation:

$$267 \quad x'_k = x_k + \eta * Uniform. \quad (11)$$

268 where *Uniform* refers a random number from uniform distribution, η is empirical coefficient and
269 0.01 was set in this study.

270 It is noteworthy that a large number of particles may lead to filter collapse, here, we set the
271 number of particles equals to 100 following references (Mechri et al., 2014; Magnusson et al., 2017;
272 Piazzzi et al., 2018). Moreover, to prevent the particle ensemble unable to represent the prior of model
273 state due to the model structurally deficient, a gaussian type model error, $N(\mu, \sigma)$, was added to the
274 ensemble members. The μ was obtained from the mean value of residual between simulation and
275 observation, and the variance σ was set to 0.01.

276 **2.4 DA experimental design**

277 **2.4.1 Perturbation of meteorological input data**

278 The accuracy of model's output largely depends on the input meteorological forcing dataset for

279 land surface models, and meteorological forcing are one of the major sources of uncertainty affecting
 280 simulation results (Raleigh et al., 2015). The precipitation and air temperature are the most important
 281 input elements for snow simulations since their roles in determining the quantity of rainfall and
 282 snowfall.

283 To produce the forcing data ensemble, the air temperature and precipitation were perturbed
 284 following the method of Lei et al. (2014). In this study, the precipitation was assumed to have an error
 285 with a log-normal distribution, and it is expressed as follows:

$$286 \quad P_t^i = \exp\left(\mu_{\ln P} + \varphi_{P,i} \cdot \sigma_{\ln P} / 2\right). \quad (12)$$

$$287 \quad \sigma_{\ln P} = \sqrt{\ln\left(\frac{(\alpha_p \cdot P_t)^2}{P_t^2} + 1\right)}. \quad (13)$$

$$288 \quad \mu_{\ln P} = \ln\left(\frac{P_t^2}{\sqrt{P_t^2 + (\alpha_p \cdot P_t)^2}}\right). \quad (14)$$

289 Where P_t and P_t^i are the observed and perturbed precipitation at time t , respectively; the log
 290 transformation of P_t^i is a Gaussian distribution with a mean ($\mu_{\ln P}$) and a standard deviation ($\sigma_{\ln P}$);
 291 α_p is the variance scaling factor of the precipitation, which was set to 0.5 in this study; and $\varphi_{P,i}$ is
 292 a normally distributed random number. Meanwhile, the ensemble of the air temperature was obtained
 293 as follows:

$$294 \quad T_t^i = T_t - \gamma(1 - 2w^i), w^i \sim U(0,1). \quad (15)$$

295 Where T_t and T_t^i are the observed and perturbed air temperatures at time t , respectively; γ
 296 is the variance scaling factor of the temperature with a value of 2.0; and w^i is the random noise with
 297 a uniform distribution between 0 and 1. An forcing ensemble containing 100 particles was obtained
 298 through above perturbation method in this study.

299 **2.4.2 Evaluation metrics**

300 In order to properly quantify the filter performance, each experiment is evaluated by statistical
 301 analysis based on the daily mean values of simulations and observations. In this study, we used the
 302 Kling-Gupta efficiency (KGE) coefficient (Gupta et al., 2009) to evaluate the filter performance,
 303 which allows the analysis of how the assimilation of snow observations succeeds in properly updating
 304 the model simulations, on average:

305
$$KGE = 1 - \sqrt{(r-1)^2 + (a-1)^2 + (b-1)^2} . \quad (16)$$

306 Where r is the linear correlation coefficient between the simulated and observed SD; a is the ratio
 307 of the standard deviation of simulated SD to the standard deviation of the observed ones; and b is the
 308 ratio of the mean of simulated SD to the mean of observed ones, here, the simulated SD is the mean
 309 SD ensemble simulations. Theoretically, when $r=1$, $a=1$ and $b=1$ in equation (16), the KGE
 310 will obtain the optimal value which equals to 1, and this illustrates that the simulated SD highly
 311 consistent with the observed ones.

312 The time series of SD obtained from assimilation scenarios was compared to observations for
 313 evaluating the performance of the assimilation, and the root-mean-square error (RMSE) was
 314 employed:

315
$$RMSE = \sqrt{\frac{1}{N} \sum_{i=1}^N (obs(i) - sim(i))^2} . \quad (17)$$

316 where N is the total number of observations, $sim(i)$ is the simulated value at time i , and $obs(i)$
 317 is the observed value at time i .

318 Another statistical index is the continuous ranked probability skill score (CRPSS), which is
 319 evaluated to assess changes to the overall accuracy of the ensemble simulations of each experiment
 320 (CRPS) by considering the open-loop ensemble control run as the reference one ($CRPS_{ref}$), and the
 321 calculation scheme is shown in the following formula:

322
$$CRPSS = 1 - \frac{CRPS}{CRPS_{ref}} . \quad (18)$$

323 where CRPS is the continuous ranked probability score which can measure the difference between
 324 continuous probability distribution and deterministic observation samples (detail in Hersbach, 2000).
 325 A smaller CRPS value indicates better probabilistic simulation and the CRPS score of a perfect
 326 simulation would equals to 0. Therefore, the changes in overall accuracy of the SD ensemble
 327 simulations can be measured by CRPSS. However, unlike the CRPS score, the optimal CRPSS score
 328 is equal to 1 and negative values indicate a negative improvement with respect to the reference control
 329 run.

330 **3. Results and discussion**

331 **3.1 Open-loop ensemble simulations**

332 In order to investigate the impact of meteorological perturbations on snow simulations, an
 333 ensemble contained 100 SD simulations derived by as many different meteorological conditions were

334 analyzed. For the sake of concision and clarity, we considered only 1 winter season for implementing
335 snow simulation experiment at each site and the results were shown in Figure 2. As shown in Figure
336 2, the possible overestimation and underestimation of SD simulations produced by the perturbation
337 forcing data were contained in the ensemble spread which are the direct consequence of perturbation
338 of the forcing data. Since the meteorological perturbations are unbiased, the nonlinearity of physical
339 processes within model is supposed to be the main reason for the uncertainty (Piazzi et al. 2018).
340 During the winter season in northern hemisphere, precipitation and air temperature are primary
341 factors which can determine the total amount of snow. As Figure 2 shows, the intervals of SD
342 ensemble are significant different at different sites though an identical meteorological perturbation
343 method was used. At some sites, like ATY, MOHE, WFJ and CDP, larger SD ensemble spreads were
344 obtained and most of SD observations were covered by the ensemble spread, in this case, high-quality
345 particles can be directly selected from the ensemble. However, at some other sites, like ROPA, SDA
346 and SASP, narrow SD ensemble spreads were obtained and the uncertainty interval of simulated SD
347 can hardly cover the observations, in this case, the so-called high-quality particles even cannot be
348 found in the ensemble and the model prior error become a prerequisite for succeed assimilation at
349 this time. Especially at ROPA site, the snow cover was extremely unstable with the result that we can
350 hardly figure out any variation rules of SD. The narrow SD ensemble spread at this site also
351 demonstrated that the precipitation and air temperature were not the main factors causing snow
352 change. According to literatures, sublimation losses at ROPA ranged from 24% to 33% of total annual
353 ablation and occurred 60% of the time during which snow was present, and high sublimation rate
354 may be the main reason for snow instability (Herrero et al., 2016; You et al., 2020a). This directly
355 leads to a perfect ensemble spread which cover all observations cannot be produced by perturbing the
356 air temperature and precipitation. Generally speaking, the ensemble produced by perturbing air
357 temperature and precipitation does not contain high-quality particles at this site. It was found that the
358 spread of SD ensembles is increased when a snowfall event occurred due to the perturbation in
359 precipitation would providing different input snow rates for model realization at all sites. Despite this,
360 we still found the simulated SD deviated from the observation seriously, like at SNQ site, the
361 maximum value of simulated SD almost half of the maximum value of observed SD. In this case, it
362 is impossible to obtain a simulated SD ensemble spread which can cover or nearly cover the
363 observation through perturbing the meteorological forcing data. On the one hand, the precipitation
364 and air temperature are not the dominant factors affecting snow cover change which lead to a
365 narrowed ensemble spread at these sites. On the other hand, though the variation trend of snow cover
366 can be accurately expressed by Noah-MP model, seriously underestimation of the simulated SD
367 shows the snow simulation performance of Noah-MP is poor at these sites. Nonetheless, the simulated
368 ensembles will be improved whenever the prior error of model state is considered.

369 *3.2 DA simulations with perturbed forcing data*

370 Generally, the ability of a model to simulate autonomously can be limited if observation data is
371 assimilated too frequently, resulting in assimilation results that are essentially the same as the
372 observations and do not reflect the differences among models. To address this, the site SD
373 measurements were assimilated into Noah-MP model with an observation frequency of five days in
374 this study, enabling the GPF to perform differently at distinct sites. Figure 3 shows the SD assimilation
375 results across snow climates, indicating a substantial improvement in the SD simulations with
376 satisfactory assimilation performance at all sites. The GPF algorithm can handle not only the seriously
377 underestimation, such as at SNQ, SDA, but also the overestimation during snow ablation period, as
378 seen at CDP, SASP, ATY and MOHE site. These results demonstrate the effectiveness of the GPF
379 algorithm as a snow data assimilation scheme and its ability to significantly improve SD simulations,
380 despite the numerous overestimations and underestimations that may occur in the Noah-MP model's
381 snow simulation results across snow climates.

382 The effectiveness of GPF in updating SD simulations is demonstrated by the KGE values of the
383 DA simulations with perturbed meteorological forcing data, as shown in Figure 4. Although the mean
384 ensemble simulations of SD exhibit substantial improvement at all sites, not all ensemble members
385 were improved as per the distribution of GPF-DA KGE values. Some ensemble members achieved
386 significant improvement at sites like SDA, SASP, MOHE and SNQ, while others showed only slight
387 improvement at sites like ATY, WFJ. Figure 4 also reveals that the update of SD model simulations
388 at ROPA and WFJ sites is more challenging. Snow simulation performance at the ROPA site is known
389 to be poor due to the high sublimation rate. Certainly, the median value of SD ensemble prediction
390 KGE values as expected below zero at this site, indicating that there are few qualified simulations in
391 the prediction ensemble. While the GPF succeeds in enhancing the SD simulations at ROPA, the
392 distribution of GPF-DA KGE values is not concentrated enough, with the 25th percentile
393 approximately at 0.2 and the 75th percentile at about 0.7, indicating that the GPF assimilation
394 algorithm cannot enhance all members but can raise the mean level and obtain an approximation of
395 the optimal posterior estimation. Conversely, the assimilation of snow measurements at CDP site
396 resulted in poor quality of the SD simulations compared to the open-loop ensemble simulations. The
397 median value of GPF-DA KGE was lower than the median value of OL KGE, indicating that a
398 considerable number of ensemble simulations failed to capture the observed values after assimilating
399 snow measurements. However, Figure 3 shows that the mean ensemble simulations after assimilating
400 snow measurements are much closer to SD observations. Thus, it underscores the importance of the
401 ensemble mean in characterizing the filter effectiveness and the approximate value of the optimal
402 posterior estimation of model state. Additionally, the scale of the model ensemble spread was found
403 to be the determinant factor that significantly affects assimilation results. A large ensemble spread
404 can adjust the simulations toward the observed system state even if the model predictions are heavily
405 biased.

406 Figure 5 displays the CRPSS value of GPF-DA at different sites. The smaller the CRPSS value,
407 the worst the probabilistic simulation (the optimal score being equal to 1). The highest CRPSS score
408 of 0.91 was achieved at SASP, while the lowest score of 0.44 was observed at CDP. These results
409 indicate that the GPF enhances the overall accuracy of ensemble simulations most at SASP and least
410 at CDP with respect to the open-loop ensemble simulation. Certainly, this cannot be illustrated by the
411 mean ensemble simulations (Figure 3) but consistent with the KGE statistical results (Figure 4).
412 Although the open-loop simulations at SNQ exhibited serious underestimation, a satisfactory
413 assimilation result was obtained at this site with a CRPSS score of 0.87. At SNQ site, the snow
414 simulation performance of Noah-MP model is poor and the model shows a serious underestimation
415 during snow stable phase, implementing data assimilation experiment in this case is a tricky business
416 since it is difficult to obtain a suitable simulated ensemble by perturbing the meteorological forcings.
417 However, since the model prior error was considered in GPF algorithm, the overall accuracy of the
418 ensemble simulations will be substantial enhanced and this is the reason why a satisfactory
419 assimilation result at SNQ site can be obtained. ROPA was found to be a difficult site to enhance the
420 overall accuracy of ensemble simulations, with a CRPSS score of only 0.58. The snow cover was
421 highly unstable and the variation of SD exhibited extreme irregularity may be the main obstacles to
422 snow data assimilation at this site.

423 Based on these findings, we conclude that the effectiveness of GPF varied among snow climates:
424 it can be employed as snow data assimilation scheme across snow climates, however, it showed
425 different performance at different sites. It is necessary to explore the sensitivity of measurement
426 frequency and ensemble size for GPF assimilation scheme across different sites.

427 ***3.3 Sensitivity analysis of DA scheme to SD measurement frequency***

428 For complex land/snow process models, model errors can gradually lead to the system deviating
429 from the true value. Therefore, it is necessary to continuously incorporate observations into the model
430 framework to adjust the operating trajectory of the state. Obviously, the frequency of incorporating
431 observations, that is, the assimilation interval, has an important impact on the assimilation system. To
432 investigate the effect of the SD measurement frequency on the performance of GPF, we conducted a
433 sensitivity experiment at eight sites. We aimed to determine how reducing the frequency of SD
434 measurements affects the DA simulations. As expected, a decrease in SD measurement frequency led
435 to a reduction in the impact of the GPF updating on the model simulations, resulting in a gradual
436 increase in the mean value of RMSE. Figure 6 illustrates the RMSE ensembles of SD simulations
437 resulting from assimilating different frequency SD measurements over the snow period at each site.
438 Higher frequency SD assimilation is beneficial in mitigating the RMSE value of simulated SD, as
439 shown by the lower RMSE value achieved when the frequency of SD measurement was set to five
440 days. This means that more frequent SD measurements improve the accuracy of the model, which is
441 particularly useful in regions where snow conditions can change rapidly. The range of RMSE values

442 at different sites varied significantly, as it was related to the maximum value of SD. For instance, a
443 thick snow at SNQ and WFJ sites during the snow period led to larger RMSEs of SD simulations.
444 Notably, an increase in the length of the assimilation window generally resulted in a significant
445 increment of the RMSE value. However, an abnormal occurrence was observed at the SDA site, where
446 the assimilation effect of 20 days of SD measurements was significantly better than that of 15 days.
447 Although the RMSE distribution of SD assimilation results with 20 days of observations appeared
448 superior to that of 15 days, the RMSE mean values of the two were very close: 0.08 m and 0.07 m,
449 respectively. Therefore, this anomaly can be ignored. These results indicate that the frequency of SD
450 observations has a significant impact on the effectiveness of the GPF algorithm and that dense
451 observation data can effectively improve the assimilation result.

452 ***3.4 Sensitivity analysis of DA scheme to ensemble size***

453 The results of the experiment aimed at evaluating the impact of particle number on the
454 assimilation performance of GPF are presented in Figure 7. As expected, increasing the particle
455 number below the threshold leads to a significant improvement in the percent effective sample size.
456 However, the filter performance does not improve significantly when the particle number exceeds the
457 threshold. Figure 7 shows that the GPF algorithm yields the minimum error at all sites when the
458 particle number is set to 100, indicating that one hundred particles can optimize the performance of
459 GPF algorithm. Although a large particle number can enhance particle diversity and prevent filter
460 divergence, it increases the computation burden without reducing the error of the system. As
461 illustrated in Figure 7, the RMSEs are generally at the same level when the particle number equals
462 120 and 160, and the RMSE are significantly larger than the RMSE when the particle number is equal
463 to 100. The slight impact of the change in the particle number on the performance of GPF, when the
464 particle number is below the threshold, indicates low system sensitivity to the ensemble size, and this
465 is observed at all sites. Essentially, increasing the particle number blindly does not guarantee a better
466 DA performance of the GPF algorithm. As demonstrated in Figure 7, the RMSEs of simulated snow-
467 depth are virtually unchanged at all sites, despite an increase in the particle number from 120 to 160.
468 This suggests that blindly increasing the ensemble size only increases the computational burden
469 without improving the performance of GPF.

470 ***3.5 Compared to traditional resampling methods***

471 To demonstrate the effectiveness of using genetic algorithms for particle resampling, we
472 compared the results of our genetic algorithm (PF-G) to those of traditional resampling methods:
473 systematic resampling (PF-S) and multinomial resampling (PF-M), both of which are commonly used
474 in particle resampling. The calculation process for these methods is detailed in the particle filter
475 introduction references. Figure 8 shows the RMSE values of SD simulations using these three
476 methods. We found that the PF-G outperforms PF-M and PF-S at all sites, as evidenced by the

477 significantly smaller mean and median RMSE values. This indicates that the PF-G is suitable for
478 snow data assimilation in different snow climates and is superior to traditional particle filters to a
479 certain extent. At most sites (MOHE, ATY, SDA, and ROPA), PF-M and PF-S showed similar
480 performance, meaning that these methods did not produce a significant difference in the assimilation
481 results. This is because these traditional resampling methods can only address particle degeneration
482 by resampling particles, but cannot prevent particle impoverishment. Therefore, they are unable to
483 select high-quality particles and keep the particles have variety. Notably, the mean and median RMSE
484 values for PF-G were significantly lower than those of PF-M and PF-S at some sites (SASP, SNQ,
485 and WFJ) where the snow cover was relatively thick, with maximum SD during the snow period
486 reaching 2.45 m, 2.95 m, and 2.40 m, respectively. This suggests that PF-G performs better in
487 assimilating data from thick snow covers.

488 **4.** The multinomial and systematic resampling methods select particles from the original particle set
489 at different levels or based on the accumulation of particle weights. Both the two resampling
490 methods extract particles from the entire particle set, and the corresponding particle values do not
491 undergo any essential changes. However, compared with the two traditional particle resampling
492 methods, genetic algorithm first uses the fitness function to calculate the "survival rate" of each
493 particle one by one, and then performs crossover, mutation and other operations on the selected
494 particles. This approach ensures that the resampled particles are high-quality particles, which is
495 the main reason why genetic particle filtering has an advantage in the snow data assimilation
496 experiments. As can be seen from Figure 8, the assimilation error by genetic particle filter is the
497 smallest one at all sites. From the results of the real assimilation experiment, it can be seen that
498 genetic particle filtering have more advantages over than other two methods.

Conclusions

499 In this study, we investigated the potential of using GPF as a snow data assimilation scheme
500 across eight sites with varying snow climates. We addressed the problem of degeneration and
501 impoverishment in PF algorithm by using the genetic algorithm to resample particles. We also
502 examined the sensitivity of GPF scheme to measurement frequency and ensemble size. The main
503 findings of this study are as follows:

- 504 1. The GPF was an effective snow data assimilation scheme and can be used across different snow
505 climates. The genetic algorithm effectively addressed the problem of particle degeneration and
506 impoverishment in PF algorithm.
- 507 2. Our experiment showed that the system has a low sensitivity to the particle number, and 100
508 particles can achieve a better assimilation result across different snow climates. This indicates
509 that 100 particles are suitable for representing the high dimensionality of the system.
- 510 3. We found that perturbations of meteorological forcing data were not sufficient to provide

511 ensemble spread, resulting in poor filter performance. Particle inflation can make up for this
512 deficiency. Moreover, we observed that the RMSE of simulated SD decreased significantly with
513 the increase of the frequency of SD measurement, indicating that dense observational data can
514 improve the assimilation results.

515 4. Compared to the two classic resampling methods, the particle filter with genetic algorithm as
516 resampling method shows a better assimilation performance especially in a thick snow cover, the
517 distribution RMSEs are more centralized and a smaller mean error will be obtained.

518 Our experiments were based on forcing data and snow observations from various sites with different
519 snow climates. While our results provide a reference for applying GPF to snow data assimilation,
520 further research is needed to investigate the performance of GPF on a regional scale and to explore
521 the assimilation of snow observational data from remote sensing or wireless sensor networks into
522 land surface model by GPF. In summary, our study demonstrates the feasibility of using GPF for snow
523 data assimilation and provides valuable insights for future research in this area.

524 **Acknowledgements**

525 This work was supported by the National Natural Science Foundation of China (grant number
526 42101361, 42130113, 41871251 and 41971326). Key Research and Development Program of Anhui
527 Province (2022107020028).

528 **References**

529 Abbasnezhadi, K., Rousseau, A. N., Foulon, E., and Savary, S.: Verification of regional deterministic
530 precipitation analysis products using snow data assimilation for application in meteorological
531 network assessment in sparsely gauged Nordic basins, *Journal of Hydrometeorology*, 22, 859-
532 876, <https://doi.org/10.1175/JHM-D-20-0106.1>, 2021.

533 Abbaszadeh, P., Moradkhani, H., Yan, H. X.: Enhancing hydrologic data assimilation by evolutionary
534 particle filter and Markov Chain Monte Carlo, *Advances in Water Resources*, 111, 192-204,
535 <https://doi.org/10.1016/j.advwatres.2017.11.011>, 2018.

536 Ahmadi, M., Mojallali, H., Izadi-Zamanabadi, R.: State estimation of nonlinear stochastic systems
537 using a novel meta-heuristic particle filter, *Swarm and Evolutionary Computation*, 4, 44-53,
538 <https://doi.org/10.1016/j.swevo.2011.11.004>, 2012.

539 Andreadis, K. M., Lettenmaier, D. P.: Assimilating remotely sensed snow observations into a
540 macroscale hydrology model, *Advances in water resources*, 29, 872-886, <https://doi.org/10.1016/j.advwatres.2005.08.004>, 2006.

542 Barnett, T. P., Adam, J. C., Lettenmaier, D. P.: Potential impacts of a warming climate on water
543 availability in snow-dominated regions, *Nature*, 438, 303-309, <https://doi.org/10.1038/nature04141>, 2005.

545 Balsamo, G., Albergel, C., Beljaars, A., Boussetta, S., Burun, E., Cloke, H., Dee, D., Dutra, E.,

- 546 Munoz-Sabater, J., Pappenberger, F., de Rosnay, P., Stockdale, T., and Vitart, F.: ERA-
547 Interim/Land: a global land surface reanalysis data set, *Hydrology and Earth System Sciences*,
548 19, 389-407, <https://doi.org/10.5194/hess-19-389-2015>, 2015.
- 549 Bergeron, J. M., Trudel, M., Leconte, R.: Combined assimilation of streamflow and snow water
550 equivalent for mid-term ensemble streamflow forecasts in snow-dominated regions, *Hydrology*
551 *and Earth System Sciences*, 20, 4375-4389, <https://doi.org/10.5194/hess-20-4375-2016>, 2016.
- 552 Che, T., Li, X., Jin, R., and Huang, C. L.: Assimilating passive microwave remote sensing data into a
553 land surface model to improve the estimation of snow depth, *Remote Sensing of Environment*,
554 143, 54-63, <https://doi.org/10.1016/j.rse.2013.12.009>, 2014.
- 555 Chen, Z.: Bayesian filtering: From Kalman filters to particle filters, and beyond, *Adaptive Systems*
556 *Laboratory Technical Report*, McMaster University, Hamilton, 25pp., 2003.
- 557 Chen, Y. Y., Yang, K., He, J., Qin, J., Shi, J. C., Du, J. Y., and He, Q.: Improving land surface
558 temperature modeling for dry land of China, *Journal of Geophysical Research-Atmospheres*,
559 116, D20104, <https://doi.org/10.1029/2011JD015921>, 2011.
- 560 Cortes, G., Giroto, M., Margulis, S.: Snow process estimation over the extratropical Andes using a
561 data assimilation framework integrating MERRA data and Landsat imagery, *Water Resources*
562 *Research*, 52, 2582-2600, <https://doi.org/10.1002/2015WR018376>, 2016.
- 563 Dee, D. P., Uppala, S. M., Simmons, A. J., Berrisford, P., Poli, P., Kobayashi, S., Andrae, U.,
564 Balsameda, M. A., Balsamo, G., Bauer, P., Bechtold, P., Beljaars, A. C. M., van de Berg, L.,
565 Bidlot, J., Bormann, N., Delsol, C., Dragani, R., Fuentes, M., Geer, A. J., Haimberger, L., Healy,
566 S. B., Hersbach, H., Holm, E. V., Isaksen, L., Kallberg, P., Koehler, M., Matricardi, M., McNally,
567 A. P., Monge-Sanz, B. M., Morcrette, J. J., Park, B. -K., Peubey, C., de Rosnay, P., Tavolato, C.,
568 Thepaut, J. N., and Vitart, F.: The ERA-Interim reanalysis: configuration and performance of the
569 data assimilation system, *Quarterly Journal of the Royal Meteorological Society*, 137, 553-597,
570 <https://doi.org/10.1002/qj.828>, 2011.
- 571 Dechant, C., Moradkhani, H.: Radiance data assimilation for operational snow and streamflow
572 forecasting, *Advances in Water Resources*, 34, 351-364, <https://doi.org/10.1016/j.advwatres.2010.12.009>, 2011.
- 574 Deschamps-Berger, C., Cluzet, B., Dumont, M., Lafaysse, M., Berthier, E., Fanise, P., Gascoin, S.:
575 Improving the Spatial Distribution of Snow Cover Simulations by Assimilation of Satellite
576 Stereoscopic Imagery, *Water Resources Research*, 58, <https://doi.org/10.1029/2021WR030271>,
577 2022.
- 578 Dettinger, M.: Climate change impacts in the third dimension, *Nature Geoscience*, 7, 166-167,
579 <https://doi.org/10.1038/ngeo2096>, 2014.
- 580 Evensen, G.: The ensemble Kalman filter: Theoretical formulation and practical implementation,
581 *Ocean Dynamics*, 53, 343-367, <https://doi.org/10.1007/s10236-003-0036-9>, 2003.
- 582 Gelb, A.: Optimal linear filtering, in: *Applied optimal estimation*, MIT Press, Cambridge, Mass, 102-
583 155, 1974.
- 584 Gordon, N. J., Salmond, D. J., Smith, A. F. M.: Novel-Approach to nonlinear non-Gaussian bayesian

- 585 state estimation, *IEE Proceedings-F Radar and Signal Processing*, 140, 107-113, <https://doi.org/10.1049/ip-f-2.1993.0015>, 1993.
- 586
- 587 Griessinger, N., Seibert, J., Magnusson, J., and Jonas, T.: Assessing the benefit of snow data
588 assimilation for runoff modeling in Alpine catchments, *Hydrology and Earth System Sciences*,
589 20, 3895-3905, <https://doi.org/10.5194/hess-20-3895-2016>, 2016.
- 590 Gupta, H. V., Kling, H., Yilmaz, K. K., and Martinez, G. F.: Decomposition of the mean squared error
591 and NSE performance criteria: Implications for improving hydrological modelling, *Journal of*
592 *Hydrology*, 377, 80-91, <https://doi.org/10.5194/10.1016/j.jhydrol.2009.08.003>, 2009.
- 593 Herrero, J., Polo, M. J., Monino, A., and Losada, M. A.: An energy balance snowmelt model in a
594 Mediterranean site, *Journal of Hydrology*, 371, 98-107, <https://doi.org/10.1016/j.jhydrol.2009.03.021>, 2009.
- 595
- 596 Herrero, J., Polo, M. J., Pimentel, R., and Pérez-Palazón, M. J.: Meteorology and snow depth at
597 Refugio Poqueira (Sierra Nevada, Spain) at 2510 m 2008-2015, *PANGEA*, 2016.
- 598 Hersbach, H.: Decomposition of the continuous ranked probability score for ensemble prediction
599 systems, *Weather and Forecasting*, 15, 559-570, [https://doi.org/10.1175/1520-0434\(2000\)015<0559:DOTCRP>2.0.CO;2](https://doi.org/10.1175/1520-0434(2000)015<0559:DOTCRP>2.0.CO;2), 2000.
- 600
- 601 Kwok, N., Fang, G., Zhou, W.: Evolutionary particle filter: resampling from the genetic algorithm
602 perspective. In: *Proceedings of International Conference on Intelligent Robots and Systems*,
603 *Shaw Conference Centre, Edmonton, Alberta, Canada, August 2-6*, pp. 2935-2940, 2005.
- 604 Kwon, Y., Yang, Z. L., Hoar, T. J., and Toure, A. M.: Improving the radiance assimilation performance
605 in estimating snow water storage across snow and land-cover types in North America, *Journal*
606 *of Hydrometeorology*, 18, 651-668, <https://doi.org/10.1175/JHM-D-16-0102.1>, 2017.
- 607 Lei, F. N., Huang, C. L., Shen, H. F., and Li, X.: Improving the estimation of hydrological states in
608 the SWAT model via the ensemble Kalman smoother: Synthetic experiments for the Heihe River
609 Basin in northwest China, *Advances in Water Resources*, 67, 32-45, <https://doi.org/10.1016/j.advwatres.2014.02.008>, 2014.
- 610
- 611 Malik, M. J., van der Velde, R., Vekerdy, Z., and Su, Z. B.: Assimilation of Satellite-Observed Snow
612 Albedo in a Land Surface Model, *Journal of Hydrometeorology*, 13, 1119-1130, <https://doi.org/10.1175/JHM-D-11-0125.1>, 2012.
- 613
- 614 Magnusson, J., Gustafsson, D., Husler, F., and Jonas, T.: Assimilation of point SWE data into a
615 distributed snow cover model comparing two contrasting methods, *Water Resources Research*,
616 50, 7816-7835, <https://doi.org/10.1002/2014WR015302>, 2014.
- 617 Margulis, S. A., Giroto, M., Cortes, G., and Durand, M.: A particle batch smoother approach to snow
618 water equivalent estimation, *Journal of Hydrometeorology*, 16, 1752-1772, <https://doi.org/10.1175/JHM-D-14-0177.1>, 2015.
- 619
- 620 Magnusson, J., Winstral, A., Stordal, A. S., Essery, R., and Jonas, T.: Improving physically based snow
621 simulations by assimilating snow depths using the particle filter, *Water Resources Research*, 53,
622 1125-1143, <https://doi.org/10.1002/2016WR019092>, 2017.
- 623 Moradkhani, H., Hsu, K. L., Gupta, H., and Sorooshian, S.: Uncertainty assessment of hydrologic

- 624 model states and parameters: Sequential data assimilation using the particle filter, *Water*
625 *Resources Research*, 41, W05012, <https://doi.org/10.1029/2004WR003604>, 2005.
- 626 Mechri, R., Otle, C., Pannekoucke, O., and Kallel, A.: Genetic particle filter application to land
627 surface temperature downscaling, *Journal of Geophysical Research-Atmospheres*, 119, 2131-
628 2146, <https://doi.org/10.1002/2013JD020354>, 2014.
- 629 Niu, G. Y., Yang, Z. L.: Effects of vegetation canopy processes on snow surface energy and mass
630 balances, *Journal of Geophysical Research-Atmospheres*, 109, D23111, <https://doi.org/10.1029/2004JD004884>, 2004.
- 632 Niu, G. Y., Yang, Z. L.: Effects of frozen soil on snowmelt runoff and soil water storage at a
633 continental scale, *Journal of Hydrometeorology*, 7, 937-952, <https://doi.org/10.1175/JHM538.1>,
634 2006.
- 635 Oaida, C. M., Reager, J. T., Andreadis, K. M., David, C. H., Levoe, S. R., Painter, T. H., Bormann, K.
636 J., Trangsrud, A. R., Giroto, M., and Famiglietti, J. S.: A high-resolution data assimilation
637 framework for snow water equivalent estimation across the western United States and validation
638 with the airborne snow observatory, *Journal of Hydrometeorology*, 20, 357-378,
639 <https://doi.org/10.1175/JHM-D-18-0009.1>, 2019.
- 640 Park, S., Hwang, J. P., Kim, E., and Kang, H. J.: A new evolutionary particle filter for the prevention
641 of sample impoverishment, *IEEE Transaction on Evolutionary Computation*, 13, 801-809,
642 <https://doi.org/10.1109/TEVC.2008.2011729>, 2009.
- 643 Parrish, M. A., Moradkhani, H., DeChant, C. M.: Toward reduction of model uncertainty: Integration
644 of Bayesian model averaging and data assimilation, *Water Resources Research*, 48, W03519,
645 <https://doi.org/10.1029/2011WR011116>, 2012.
- 646 Piazzzi, G., Campo, L., Gabellani, S., Castelli, F., Cremonese, E., di Cella, U. M., Stevenin, H., and
647 Ratto, S. M.: An EnKF-based scheme for snow multivariable data assimilation at an Alpine site,
648 *Journal of Hydrology and Hydromechanics*, 67, 4-19, <https://doi.org/10.2478/joh-h-2018-0013>,
649 2019.
- 650 Piazzzi, G., Thirel, G., Campo, L., and Gabellani, S.: A particle filter scheme for multivariate data
651 assimilation into a point-scale snowpack model in an Alpine environment, *Cryosphere*, 12, 2287-
652 2306, <https://doi.org/10.5194/tc-12-2287-2018>, 2018.
- 653 Pulliainen, J., Luojus, K., Derksen, C., Mudryk, L., Lemmetyinen, J., Salminen, M., Ikonen, J., Takala,
654 M., Cohen, J., Smolander, T., and Norberg, J.: Patterns and trends of Northern Hemisphere snow
655 mass from 1980 to 2018, *Nature*, 581, 294-298, <https://doi.org/10.1038/s41586-020-2258-0>,
656 2020.
- 657 Rautiainen, K., Lemmetyinen J., Schwank, M., Kontu, A., Menard, C. B., Matzler, C., Drusch, M.,
658 Wiesmann, A., Ikonen, J., and Pulliainen, J.: Detection of soil freezing from L-band passive
659 microwave observations, *Remote Sensing of Environment*, 147, 206-218, <https://doi.org/10.1016/j.rse.2014.03.007>, 2014.
- 661 Raleigh, M. S., Lundquist, J. D., Clark, M.P.: Exploring the impact of forcing error characteristics on
662 physically based snow simulations within a global sensitivity analysis framework, *Hydrology*
663 *and Earth System Sciences*, 19, 3153-3179, <https://doi.org/10.5194/hess-19-3153-2015>, 2015.

- 664 Rings, J., Vrugt, J. A., Schoups, G., Huisman, J. A., and Vereecken, H.: Bayesian model averaging
665 using particle filtering and Gaussian mixture modeling: Theory, concepts, and simulation
666 experiments, *Water Resources Research*, 48, W05520, <https://doi.org/10.1029/2011WR011607>,
667 2012.
- 668 Smyth, E. J., Raleigh, M. S., Small, E. E.: Improving SWE estimation with data assimilation: the
669 influence of snow depth observation timing and uncertainty, *Water Resources Research*, 56,
670 e2019WR026853, <https://doi.org/10.1029/2019WR026853>, 2020.
- 671 Sturm, M., Holmgren, J., Liston, G. E.: A seasonal snow cover classification system for local to global
672 applications, *Journal of Climate*, 8, 1261-1283, [https://doi.org/10.1175/1520-0442\(1995\)008<1](https://doi.org/10.1175/1520-0442(1995)008<1261:ASSCCS>2.0.CO;2)
673 [261:ASSCCS>2.0.CO;2](https://doi.org/10.1175/1520-0442(1995)008<1261:ASSCCS>2.0.CO;2), 1995.
- 674 Su, H., Yang, Z. L., Niu, G. Y., and Dickinson, R. E.: Enhancing the estimation of continental-scale
675 snow water equivalent by assimilating MODIS snow cover with the ensemble Kalman filter,
676 *Journal of Geophysical Research-Atmospheres*, 113, D08120, [https://doi.org/10.1029/2007JD00](https://doi.org/10.1029/2007JD009232)
677 [9232](https://doi.org/10.1029/2007JD009232), 2008.
- 678 Snyder, C.: Particle filters, the optimal proposal and high-dimensional systems, ECMWF Seminar on
679 Data Assimilation for Atmosphere and Ocean, pp. 6-9, Reading, U. K., 2011.
- 680 Takala, M., Luoju, K., Pulliainen, J., Derksen, C., Lemmetyinen, J., Karna, J. P., Koskinen, J., and
681 Bojkov, B.: Estimating northern hemisphere snow water equivalent for climate research through
682 assimilation of space-borne radiometer data and ground-based measurements, *Remote Sensing*
683 *of Environment*, 115, 3517-3529, <https://doi.org/10.1016/j.rse.2011.08.014>, 2011.
- 684 Trujillo, E., Molotch, N.P.: Snowpack regimes of the Western United States, *Water Resources*
685 *Research*, 50, 5611-5623, <https://doi.org/10.1002/2013WR014753>, 2014.
- 686 Van Leeuwen, P. J.: Nonlinear data assimilation in geosciences: An extremely efficient particle filter,
687 *Quarterly Journal of the Royal Meteorological Society*, 136, 1991-1999, [https://doi.org/](https://doi.org/10.1002/qj.699)
688 [10.1002/qj.699](https://doi.org/10.1002/qj.699), 2010.
- 689 Wayand, N. E., Massmann, A., Butler, C., Keenan, E., Stemberis, J., and Lundquist, J. D.: A
690 meteorological and snow observational data set from Snoqualmie Pass (921 m), Washington
691 Cascades, USA, *Water Resources Research*, 51, 10092-10103, [https://doi.org/10.1002/2015WR](https://doi.org/10.1002/2015WR017773)
692 [017773](https://doi.org/10.1002/2015WR017773), 2015.
- 693 Weerts, A. H., El Serafy, G. Y. H.: Particle filtering and ensemble Kalman filtering for state updating
694 with hydrological conceptual rainfall-runoff models, *Water Resources Research*, 42, W09403,
695 <https://doi.org/10.1029/2005WR004093>, 2006.
- 696 Wever, N., Schmid, L., Heilig, A., Eisen, O., Fierz, C., and Lehning, M.: Verification of the multi-
697 layer SNOWPACK model with different water transport schemes, *The Cryosphere*, 9, 2271-
698 2293, <https://doi.org/10.5194/tc-9-2271-2015>, 2015.
- 699 Yang, J. M., Li, C. Z.: Assimilation of D-InSAR snow depth data by an ensemble Kalman filter,
700 *Arabian Journal of Geosciences*, 14, 1-14, <https://doi.org/10.1007/s12517-021-06699-y>, 2021.
- 701 You, Y. H., Huang, C. L., Yang, Z. L., Zhang, Y., Bai, Y. L., and Gu, J.: Assessing Noah-MP
702 parameterization sensitivity and uncertainty interval across snow climates, *Journal of*

703 Geophysical Research-Atmospheres, 125, e2019JD030417, <https://doi.org/10.1029/2019JD030>
704 417, 2020.

705 Zhang, T. J.: Influence of the seasonal snow cover on the ground thermal regime: An overview,
706 *Reviews of Geophysics*, 43, RG4002, <https://doi.org/10.1029/2004RG000157>, 2005.

707 Zhu, G. F., Li, X., Ma, J.Z., Wang, Y. Q., Liu, S. M., Huang, C. L., Zhang, K., and Hu, X. L.: A new
708 moving strategy for the sequential Monte Carlo approach in optimizing the hydrological model
709 parameters, *Advances in Water Resources*, 114, 164-179, [https://doi.org/10.1016/j.advwatres.](https://doi.org/10.1016/j.advwatres.2018.02.007)
710 2018.02.007, 2018.

711

712

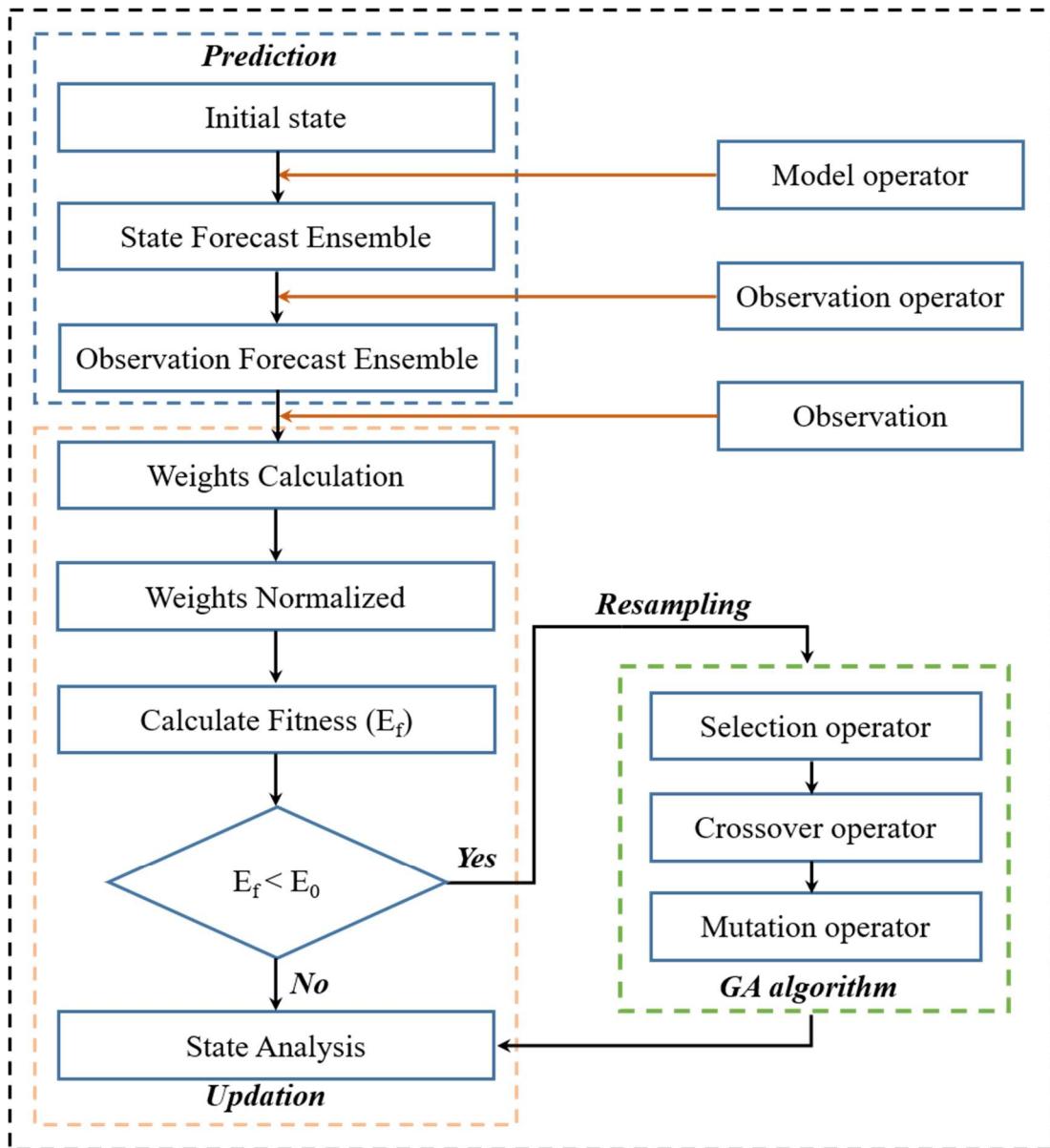
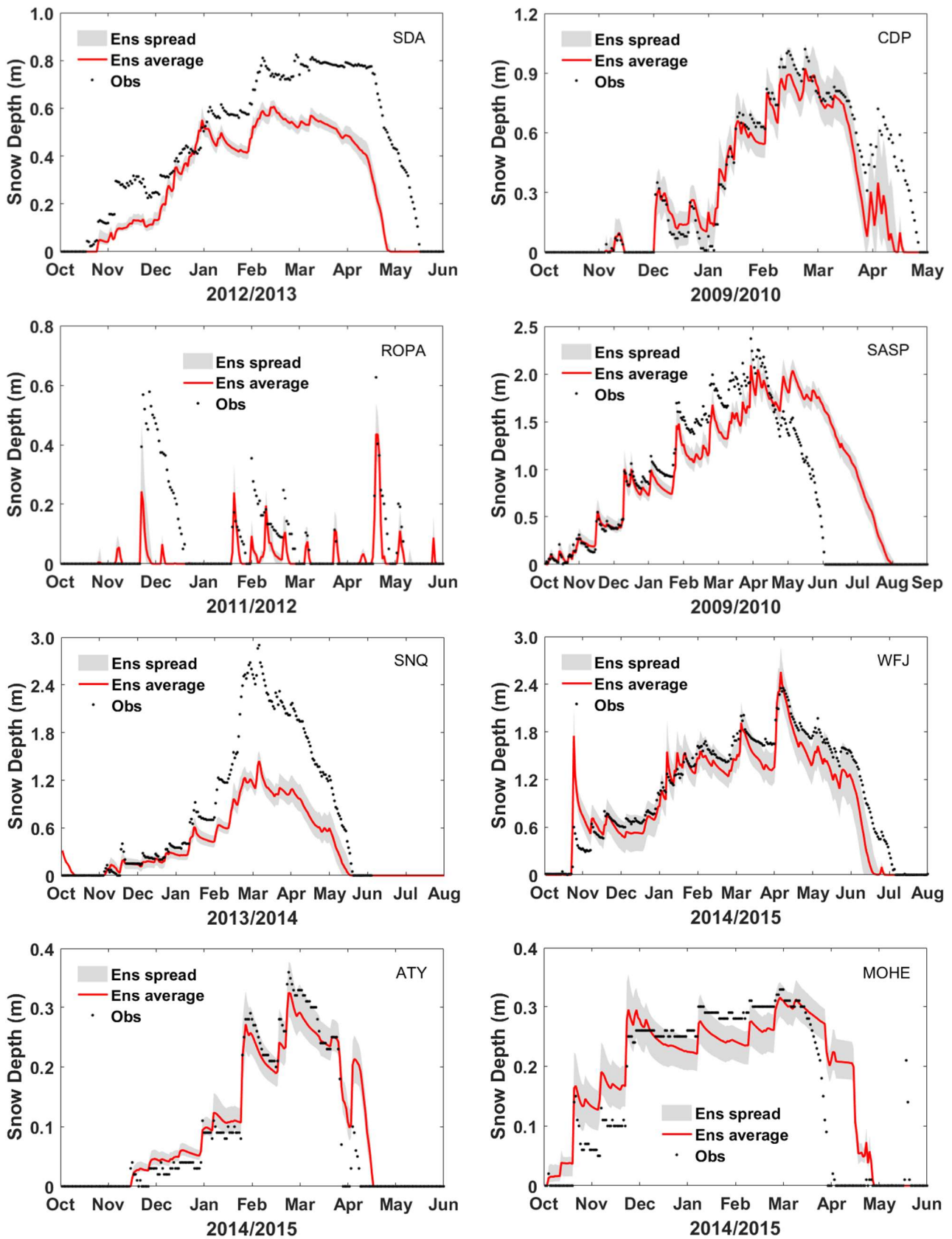


Figure 1. Flowchart of Genetic particle filter

713

714

715

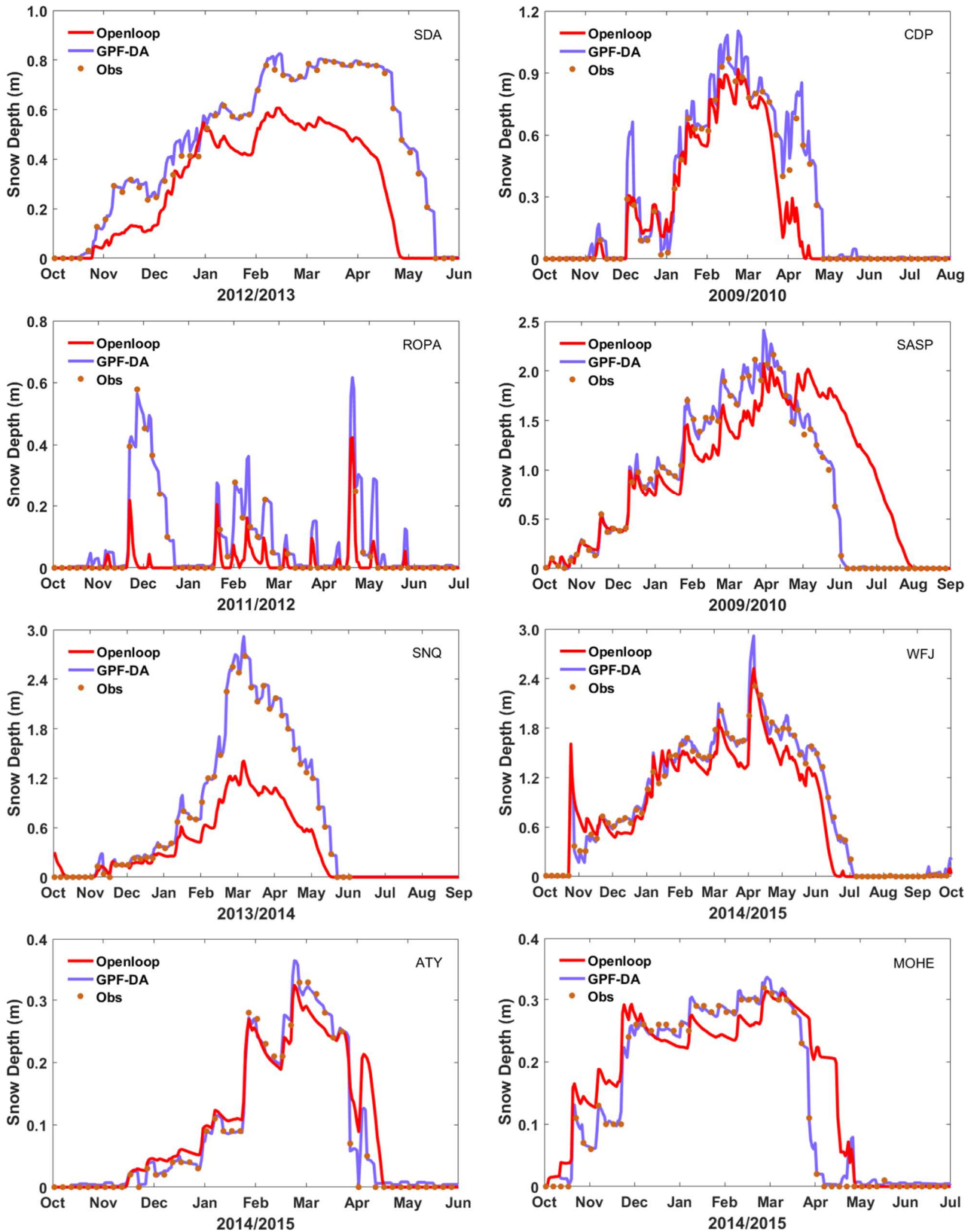


716

717

718

Figure 2. Impact of the meteorological uncertainty on snow depth ensemble simulations

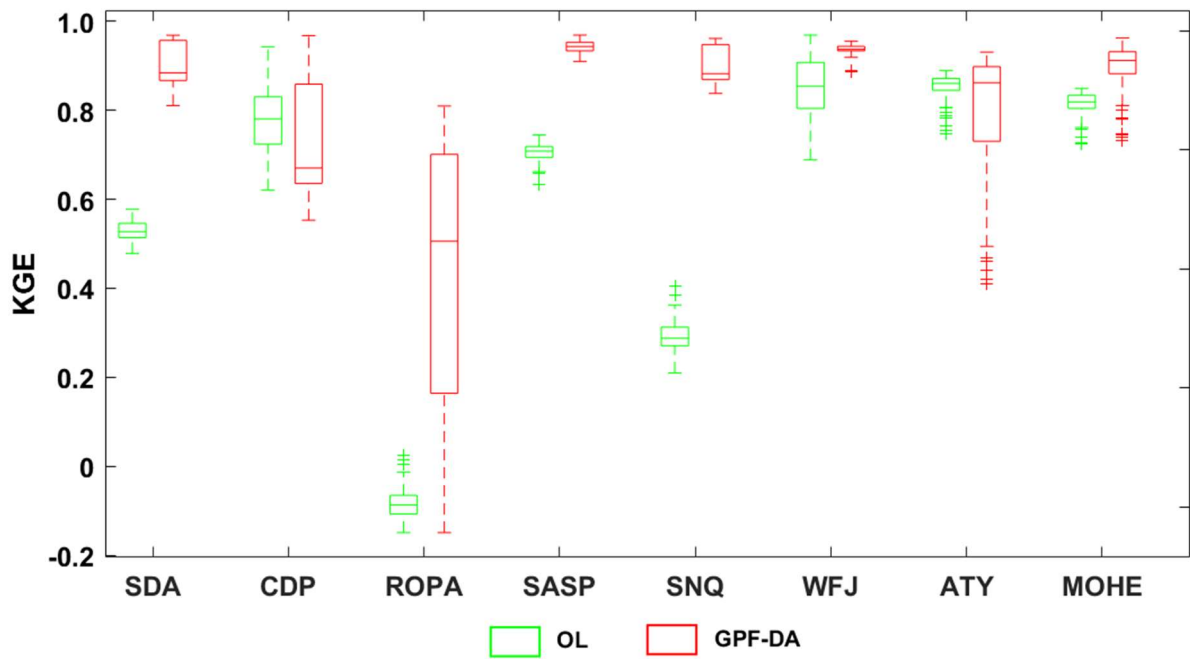


719

720 **Figure 3.** Evaluation of the SD at eight sites from mean ensemble simulation and assimilation with
 721 the measurements.

722

723

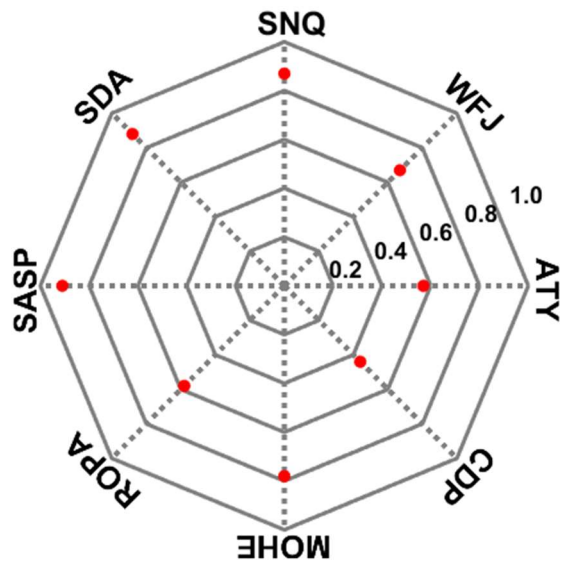


724

725 **Figure 4.** The KGE values of SD simulations, the OL and GPF-DA are in green, red, respectively.

726 The bottom and top edges of each box indicate the 25th 75th percentiles, respectively. The line in the
 727 middle of each box is the median.

728

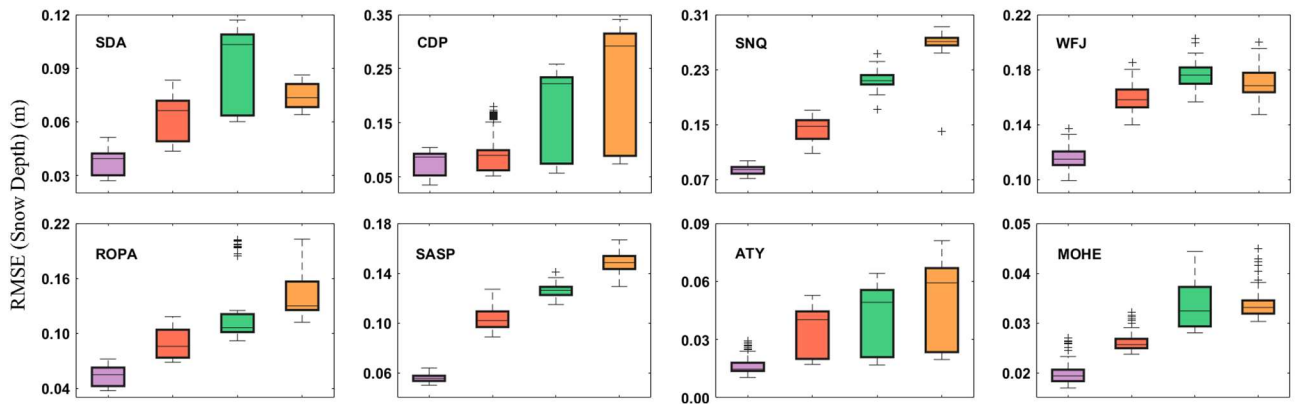


729

730

Figure 5. Comparison of the CRPSS value of GPF-DA at different sites.

731



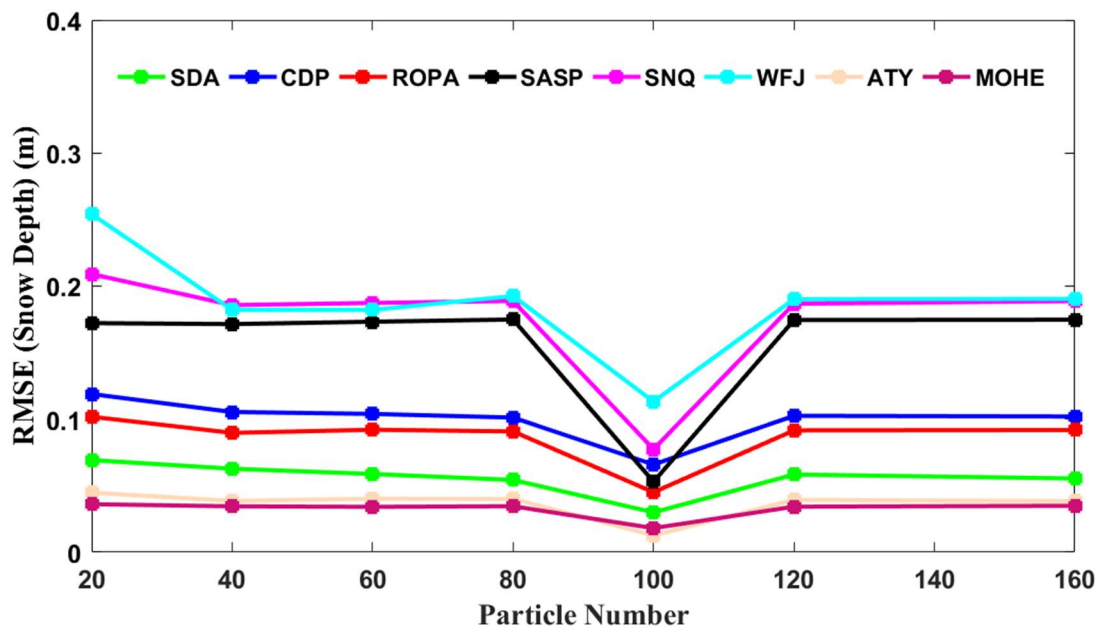
732

733

734

735

Figure 6. The RMSE values of SD simulations at different sites, from left to right in each subfigure are the assimilation observation frequency is 5, 10, 15, 20 days, respectively, and with different colors.

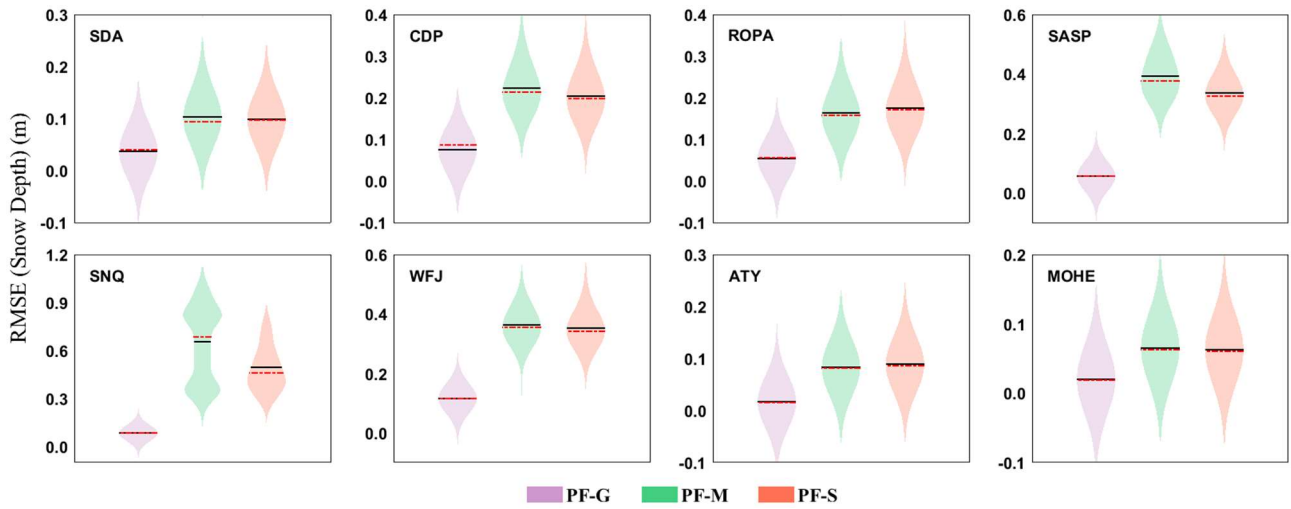


736

737 **Figure 7.** Sensitivity analysis of the GPF snow DA scheme to particle number at eight sites, during

738 different snow periods.

739



740

741 **Figure 8.** The RMSE values of SD simulations by three different resampling methods. For each
 742 subfigure, from left to right are the particles resampled by genetic algorithm, multinominal method,
 743 systematic method, respectively, and with different colors, the black line indicates the mean, and the
 744 red line indicates the median; the kernel bandwidth was 0.05.

745